Geophys. J. R. astr. Soc. (1986) **86**, 767–787

Upper mantle velocity structure estimated from *PS*-converted wave beneath the north-eastern Japan Arc

Toru Matsuzawa, Norihito Umino, Akira Hasegawa and Akio Takagi *Observation Centre for Earthquake Prediction, Faculty of Science, Tohoku University, Sendai 980, Japan*

Accepted 1986 February 11. Received 1986 January 27; in original form 1985 May 7

Summary. The upper boundary of the descending oceanic plate is located by using *PS*-waves (converted from *P* to *S* at the boundary) in the Tohoku District, the north-eastern part of Honshu, Japan. The observed *PS*–*P* time data are well explained by a two-layered oceanic plate model composed of a thin low-velocity upper layer whose thickness is less than 10 km and a thick high-velocity lower layer; the upper and lower layers respectively have 6 per cent lower and 6 per cent higher velocity than the overriding mantle. The estimated location of the upper boundary is just above the upper seismic plane of the double-planed deep seismic zone. This result indicates that events in the upper seismic plane, at least in the depth range from 60 to 150 km, occur within the thin low-velocity layer on the surface of the oceanic plate.

Key words: upper mantle structure, converted wave, low-velocity layer, subduction zone

1 Introduction

In order to locate the upper boundary of the descending oceanic plate (UBP), Okada (1971) has proposed an elegant method using the *ScSp*-phase (converted from *ScS* to *P* at the boundary). This method is now widely used to investigate the upper mantle velocity structure (e.g. Snoke, Sacks & Okada 1977; Nakanishi 1980; Nakanishi, Suyehiro & Yokota 1981).

In the Tohoku District, the north-eastern part of Honshu, Japan, Hasegawa, Umino & Takagi (1978b) located the UBP from *ScSp*-phases by using the ray tracing method. They conclude that the upper seismic plane of the double-planed deep seismic zone coincides with the UBP. Their result is valid below about 100 km depth (on the western side of the volcanic front) and it is necessary to confirm that the upper seismic plane coincides with the UBP even in the shallower part of the upper mantle.

Unless the ocean bottom seismograph (OBS) detects the *ScSp*-phase, it is impossible to locate the UBP above 100 km depth in the Tohoku District by using the *ScSp*-phase. An

Downloaded from https://academic.oup.com/gji/article/86/3/767/614858 by U.S. Department of Justice user on 17 August 2022

OBS cannot be operated for long times, and the nearby deep earthquakes from which we can observe *ScSp*-phase seldom occur. We must use a different method to locate the shallower part of the UBP.

A conspicuous phase is frequently found between *P*- and *S*-waves in the seismograms of intermediate-depth earthquakes recorded at the eastern stations of the Tohoku University seismic network. In this paper, we ascertain that this *X*-phase is a *PS*-wave converted at the UBP, and investigate the velocity structure of the upper mantle by using the *PS*–*P* time.

2 *X*-phase observed on the eastern side of the volcanic front

An example of the seismogram of the prominent *X*-phase is shown in Fig. 1. Seismometers used here are of 1 Hz velocity type. This *X*-phase has some characteristics as follows.

(1) This phase is considerably polarized and the *SV* component is dominant (Fig. 2).

(2) This phase incidents to the ground surface almost vertically on condition that this phase propagates to the ground surface as an *SV*-wave (Fig. 2).

(3) The *X*–*P* time is almost constant at each station regardless of the change of the *S*–*P* time (Fig. 3) and that of the focal depth (Fig. 4).

(4) Eastern stations have shorter *X*–*P* times than western stations (Fig. 4).

(5) The *X*–*P* time for the events in the lower seismic plane is shorter than that for the events in the upper seismic plane (Fig. 4).

(6) This phase is not observed at stations on the western side of the volcanic front (Fig. 5).

(7) This phase has large amplitude: about a half of the amplitude of *P*-wave at the maximum (Fig. 1).

The features (1) and (2) show that this phase is a converted wave from *P* to *S* at some boundary between hypocentres and stations. Feature (3) indicates the boundary is located near the stations; and (4) probably indicates the boundary is dipping westward. Phases converted or reflected more than two times with subcritical incident angle are too weak to be observed frequently. On the other hand, no post-critical reflection of *P*-waves is likely to occur at any known velocity boundary between stations and hypocentres in the deep seismic zone. The possible interpretation for this phase is considered to be one of the following:

(a) *P* – converted *S*.

(b) *P* – reflected *P* – converted *S*.

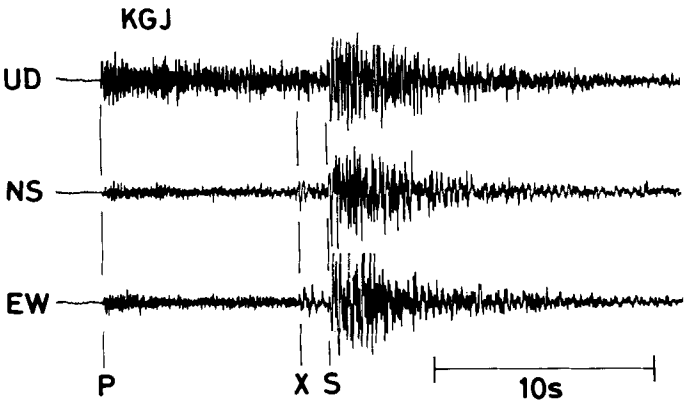

Figure 1. An example of the *X*-phase observed at KGJ. The *X*-phase is clearly seen in the horizontal components.

Downloaded from https://academic.oup.com/gji/article/86/3/767/614858 by U.S. Department of Justice user on 17 August 2022

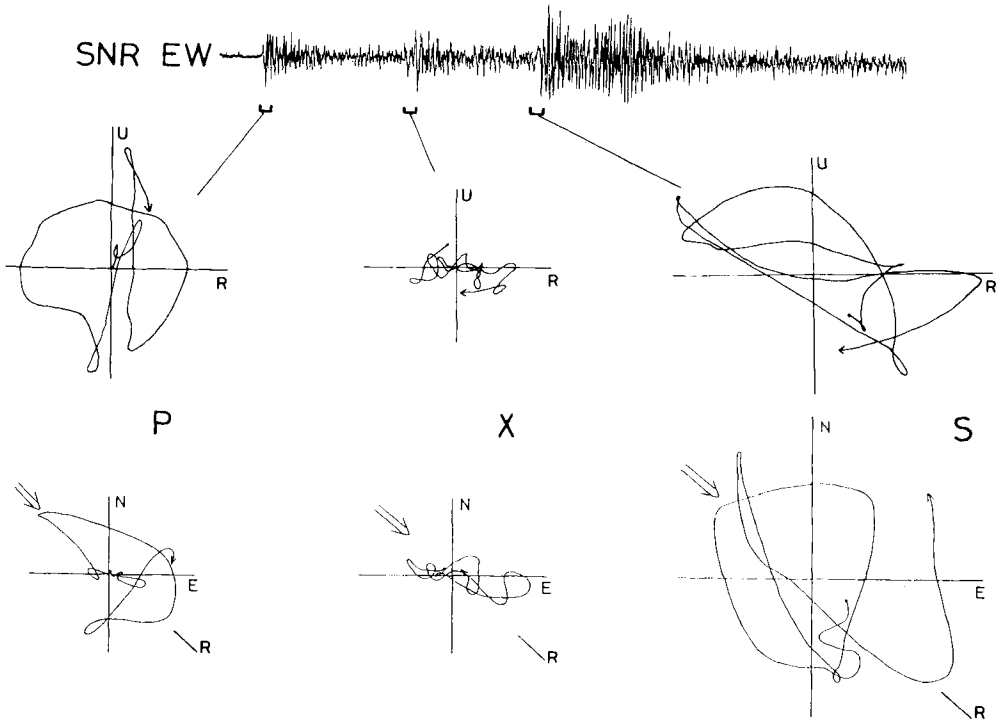

Figure 2. Particle motion of *P*-, *X*- and *S*-waves observed at SNR. Arrows represent the incident direction expected from the location of the earthquake. U. R, N and E indicate upward, radial, northward and eastward directions, respectively.

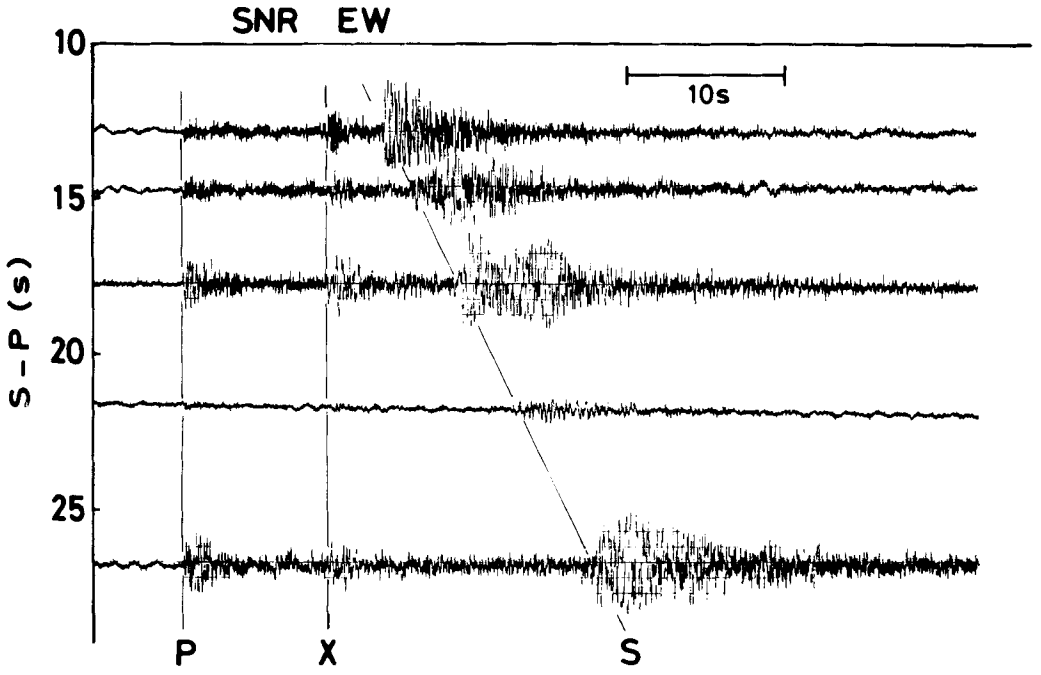

Figure 3. Examples of the records of the *X*-phase observed at SNR. The *X*–*P* time does not change with the *S*–*P* time very much.

Downloaded from https://academic.oup.com/gji/article/86/3/767/614858 by U.S. Department of Justice user on 17 August 2022

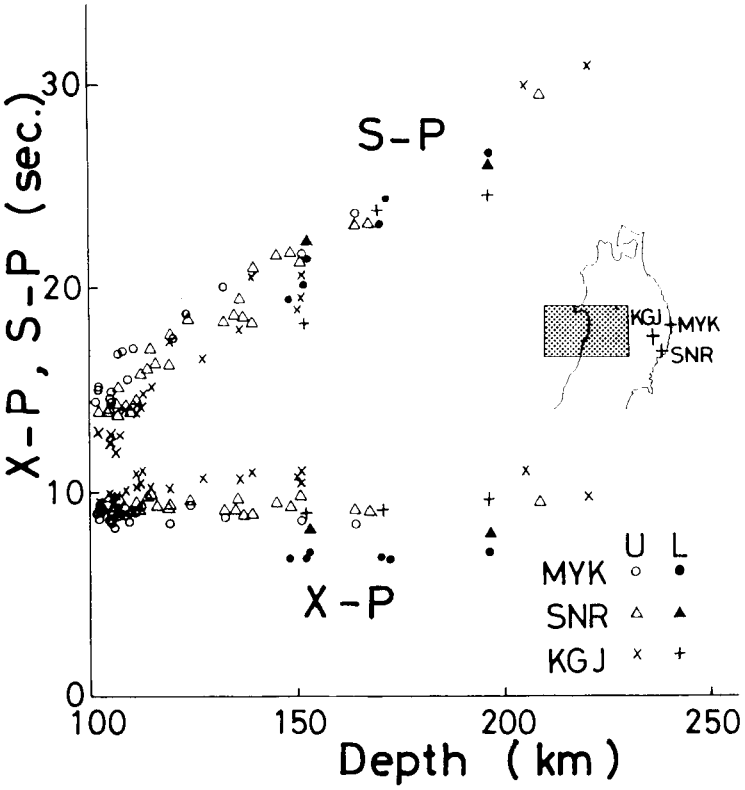

Figure 4. *X*–*P* and *S*–*P* times versus focal depth for events in the region shown in the inserted map. ○, △ and × denote the observed values at MYK, SNR and KGJ respectively for the events in the upper seismic plane. ●, ▲ and + are those for the events in the lower seismic plane.

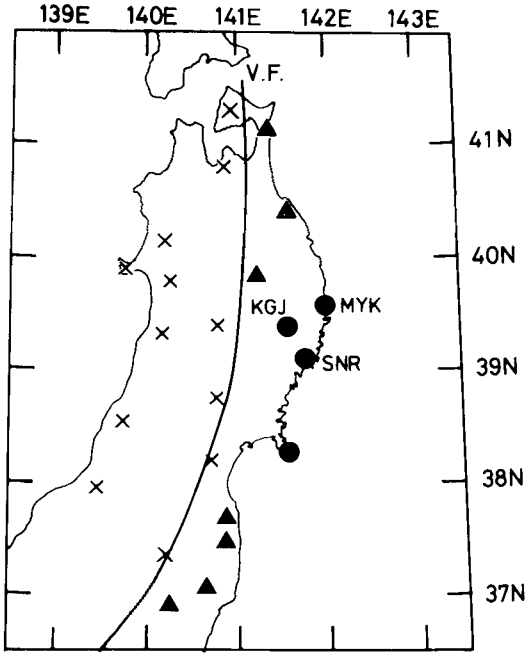

Figure 5. Map showing the stations at which the *X*-phases are observed (solid symbols). Solid circles represent the locations of the stations at which the *X*-phases are observed very frequently, and solid triangles show those at which the phases are observed but not so frequently. The stations at which the phases cannot be observed are shown by crosses.

Downloaded from https://academic.oup.com/gji/article/86/3/767/614858 by U.S. Department of Justice user on 17 August 2022

(c) P – converted S – reflected S.

(d) S – converted P – converted S.

The ray paths for these converted or reflected waves are shown in Fig. 6. Although many other ray paths can be imagined, only the probable paths are shown in this figure taking the observed value of the X–P time and the locations of the known velocity boundaries into consideration. If one among cases (ii), (iii), (iv) and (v) in Fig. 6 is the true ray path of the X-phase, a *PPP*- or *PP*-phase must also be observed before the X-phase with an amplitude larger than or nearly equal to that of the X-phase. If case (vii) or (viii) is correct, an *SP*- and *PS*-phase must be observed. However, we cannot see any clear phase with amplitudes larger than or nearly equal to that of the X-phase between the P- and the X-phases in the seismogram of any event in the upper seismic plane. Sometimes a phase is observed at about 3 s after the P-wave arrival in vertical component seismograms for events in the lower seismic plane. This phase is interpreted as an *SP*-wave (converted from an S- to a P-wave at the UBP) because only this interpretation can explain the fact that this phase cannot be found in the seismograms for the events in the upper seismic plane: if the upper seismic plane is close to the UBP, the *SP*-wave is masked by the coda of the P-wave in seismograms for events in the upper seismic plane. If case (vi) in Fig. 6 is correct, the *SPS*–P time for the event in the

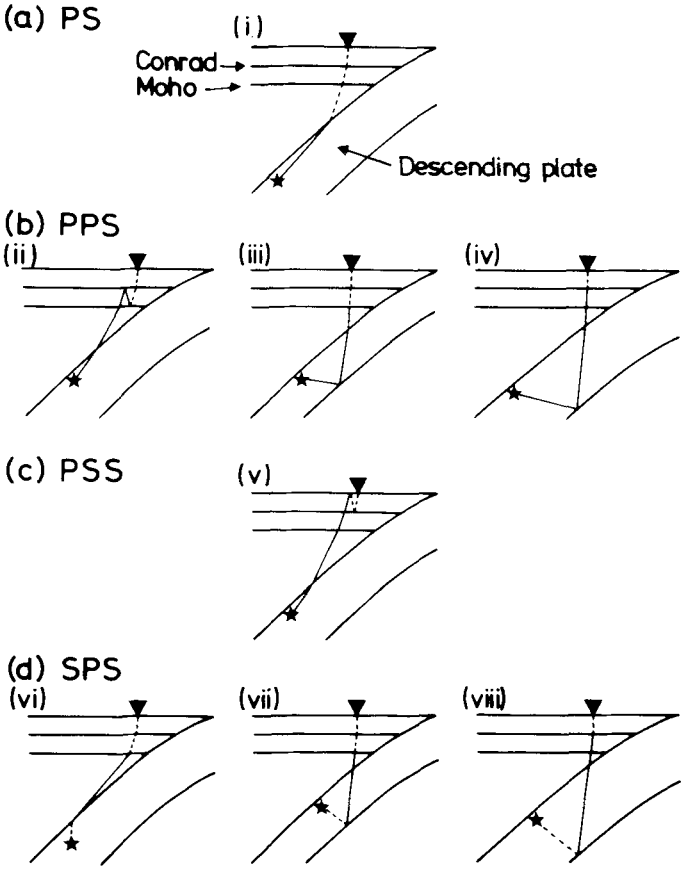

Figure 6. Possible ray paths for the X-phase projected on the vertical section. Only the known velocity boundaries are taken into consideration. Solid and dashed lines denote P- and S-waves, respectively. Triangles and stars denote stations and hypocentres.

Downloaded from https://academic.oup.com/gji/article/86/3/767/614858 by U.S. Department of Justice user on 17 August 2022

upper seismic plane should be shorter than that in the lower seismic plane. This trend is inconsistent with the observation (feature (5)).

If the ray path (i) is correct, this ray must pass through the overlying thick low-Q mantle as an SV-wave to reach the stations on the western side of the volcanic front (Hasegawa *et al.* 1979). Thus the amplitude of this phase is expected to become too weak to be observed at these stations; this trend is consistent with the feature (6). On the eastern side of the volcanic front, this phase is expected to have sufficient amplitude, taking the incident angle at the UBP into consideration. Therefore only case (i) (the PS-phase) in Fig. 6 can explain all the observed features of the X-phase. If the X-phase is the PS-phase as shown Fig. 6(a), the difference in arrival time $T_{PS} - T_P$ is a good measure of the depth to the UBP. Thus, we can locate the UBP by inversion using the $T_{PS} - T_P$ time data.

In the remainder of this paper, we assume that the X-phase is a PS-phase converted at the UBP, and investigate the velocity structure of the upper mantle.

3 One-layered oceanic plate model

We adopt the same method to locate the UBP as that developed by Horiuchi, Ishii & Takagi (1982). This method is very useful if a velocity boundary is gently curved. An outline of the method is described in the Appendix. In this study, the assumed velocity structure above the descending oceanic plate is the same as the structure which is used for locating earthquakes by the seismic network of Tohoku University (Fig. 7) (Hasegawa, Umino & Takagi 1978a). Hypocentres used here are determined by the routine of Tohoku University and are fixed in the inversion.

Many authors reported that the P-wave velocity contrast between the oceanic plate and the overlying mantle is 3–8 per cent. In this section, it is assumed that the P-wave velocity in the descending oceanic plate is 6 per cent higher than in the overlying mantle (plate model 1 in Fig. 7). Moreover, two other velocity models for the descending plate are also used for inversion (plate models 2 and 3 in Fig. 7).

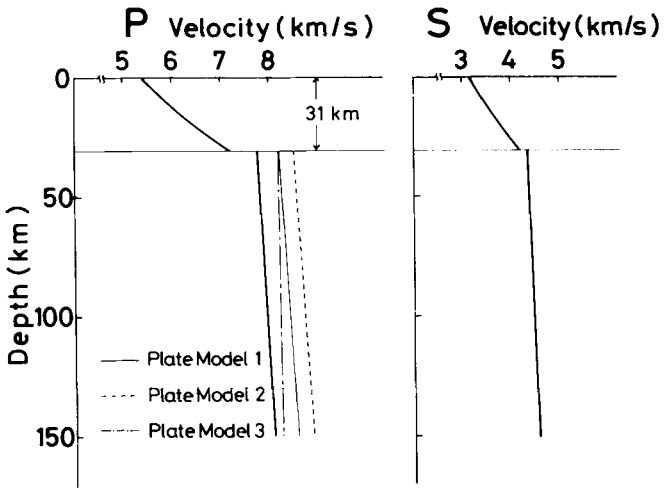

Figure 7. Velocity structures used for the location of the UBP. Thick lines denote the velocity structure for the overlying mantle. The plate model 1 (thin line) is assumed for the velocity structure within the oceanic plate. The plate models 2 (dashed line) and 3 (dot–dash line) are also used for the inversion.

Downloaded from https://academic.oup.com/gji/article/86/3/767/614858 by U.S. Department of Justice user on 17 August 2022

The data used in this section are the *PS–P* time observed at MYK, SNR and KGJ (Fig. 8) from 1977 January to 1982 February; the size of the events is $1.8 < M < 4.2$. The seismometers are of the 1 Hz velocity type and we read the *PS–P* time from paper records whose recording speed is 25 mm s^{-1}. The number of the events used and the readings are 107 and 181, respectively. The reading error of the *PS–P* time is estimated to be about 0.3 s. The epicentral distribution of the events used is shown in Fig. 8. It is appropriate that the number of the unknown parameters is approximately the same as the number of the stations (Horiuchi *et al.* 1982). Therefore in this section, the depth of the UBP (h_P) is assumed to be expressed as

$$h_P = C_0 + C_1\phi'_P + C_2\lambda'_P, \tag{1}$$

where $\phi'_P = \phi_P - 39.3°$ and $\lambda'_P = \lambda_P - 141.8°$, ϕ_P and λ_P are the latitude and longitude of a point on the UBP, respectively. Then, we estimate C_0, C_1 and C_2 iteratively (see Appendix).

The location of the UBP obtained by the inversion is shown in Fig. 9. The results obtained by using different velocity structures are also shown in the figure. The UBP obtained here roughly coincides with the upper plane of the double-planed deep seismic zone. If we look in more detail, the UBP is located just beneath the upper seismic plane. This result is inconsistent with our assumption, although the events used in the inversion are below the UBP extrapolated from the result shown in Fig. 9.

The comparison of the observed *X–P* time and the calculated *PS–P* time is shown in Fig. 10. The general pattern of the calculated *PS–P* time is the same as that of the observed *X–P* time distribution except that the observed *X–P* time is, on average, about 1 s shorter than the calculated *PS–P* time for the events in the lower seismic plane (solid circles in Fig.

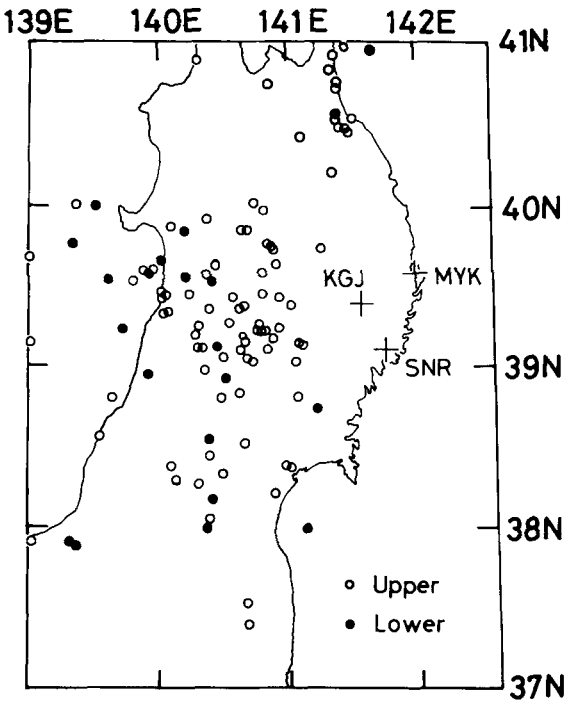

Figure 8. Epicentre distribution of the events used for the inversion (circles) and locations of stations (crosses). Open and solid circles denote the events in the upper and the lower seismic planes, respectively.

Downloaded from https://academic.oup.com/gji/article/86/3/767/614858 by U.S. Department of Justice user on 17 August 2022

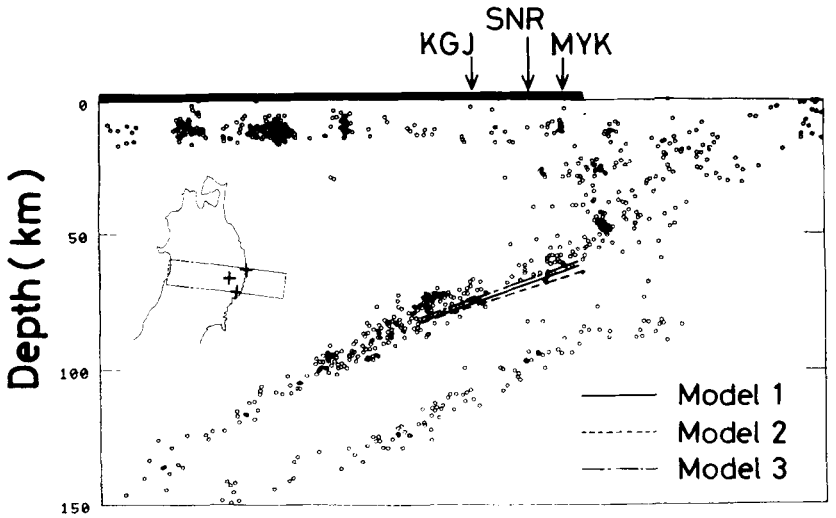

Figure 9. Estimated location of the UBP projected on to the vertical seismic section. The oceanic plate is assumed to have the single-layered structure. The locations of the seismic stations used and the land area are shown by arrows and thick line, respectively.

10). It is clear that the observed $X-P$ time for the events in the lower seismic plane is shorter than that for the events in the upper seismic plane; this feature is not so clear in the calculated $PS-P$ time distribution. Even if the velocity of the oceanic plate is assumed to be any other value, this feature cannot be explained fully.

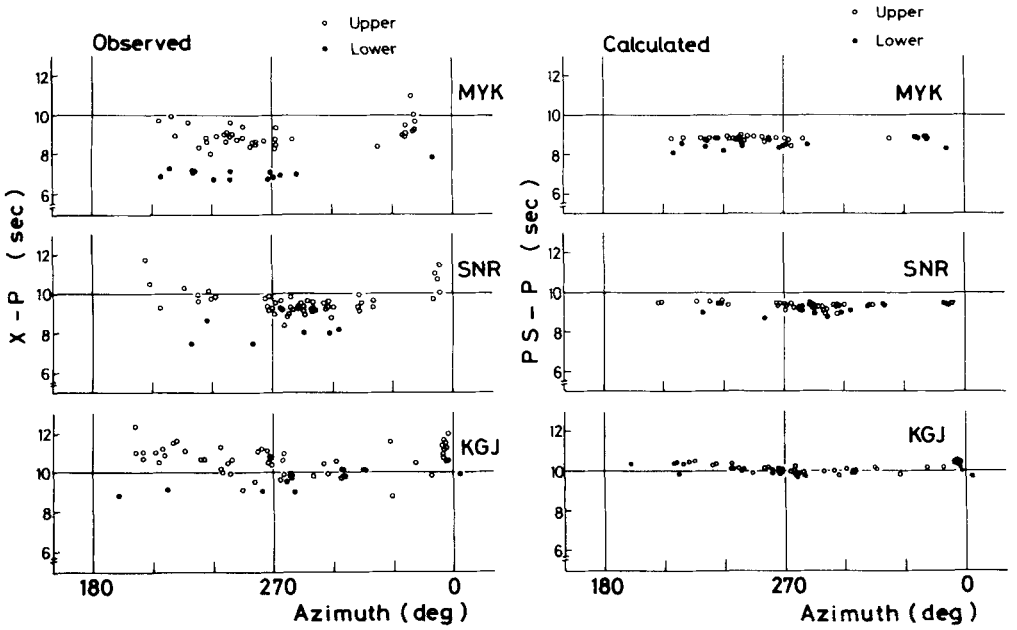

Figure 10. Observed $X-P$ time (a) and calculated $PS-P$ time (b) plotted against the azimuth from the stations to the hypocentres. Azimuths are measured clockwise from the north. Open and solid circles indicate the events in the upper and lower seismic planes.

Downloaded from https://academic.oup.com/gji/article/86/3/767/614858 by U.S. Department of Justice user on 17 August 2022

As the most probable velocity model that explains this feature, we introduce the two-layered oceanic plate model composed of low-velocity upper layer and high-velocity lower layer. In the next section, we examine whether this model can explain the feature mentioned above.

4 Two-layered oceanic plate model

If the oceanic plate has two-layered velocity structure, the ray paths of the *PS*-waves before the conversion are mostly within the upper layer of the oceanic plate for the events in the upper seismic plane, and mostly within the lower layer for those in the lower seismic plane. Therefore, the *PS–P* times for the events in the upper and the lower seismic planes are expected to reflect the velocity in the upper and the lower layers, respectively.

In order to estimate roughly the velocity contrast (fractional perturbation from the velocity in the overlying mantle) for the upper and the lower layers of the two-layered velocity structure, we locate the UBP by using the events in the two seismic planes separately with various values of the velocity contrast. Fig. 11(a) shows the standard deviation of the *PS–P* time residual in the separate inversion. For the events in the lower seismic plane, about 4 per cent velocity contrast is the most suitable. On the contrary, about

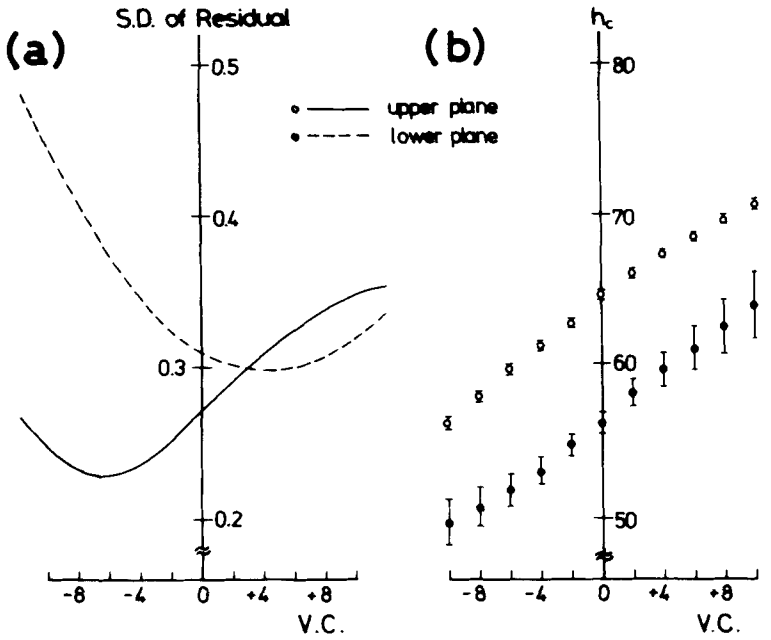

Figure 11. The results of the inversion by using the *PS–P* time. The events in the upper seismic plane and those in the lower plane are individually used for the inversion. The inversion was made with various values of the velocity contrast (VC), where VC is

$$VC = \left[\frac{\text{velocity in the oceanic plate}}{\text{velocity in the overlying mantle}} - 1 \right] \times 100.$$

(a) Standard deviation of the *PS–P* time residual. The solid and dashed lines are those obtained by using the events in the upper and lower seismic planes, respectively. (b) Estimated depth of the UBP (h_c) at the centre of the three stations used (39.3°N, 141.8°E). Open and solid circles denote the results obtained by using the events in the upper and lower planes, respectively. Error bars represent the standard deviations of the estimated depth.

Downloaded from https://academic.oup.com/gji/article/86/3/767/614858 by U.S. Department of Justice user on 17 August 2022

−6 per cent velocity contrast is the most appropriate for the events in the upper seismic plane. Moreover, the depths to the UBP at the centre of the three stations (39.3°N, 141.8°E) in both cases are almost the same and are about 60 km (Fig. 11b).

The −6 per cent velocity contrast for the upper layer is an unexpectedly low value. If the low-velocity layer is thicker than about 10 km, this layer could be detected by another kind of inversion method (e.g. Hasemi, Ishii & Takagi 1984). Therefore the low-velocity layer must be very thin: less than 10 km. In this section, we assume:

(1) the thickness of the low-velocity layer is 5 km,

(2) the inner boundary between upper and lower layers is parallel to the UBP,

(3) the earthquakes in the upper seismic plane occur within this thin low-velocity layer and

(4) the ray path of the *PS*-wave before the conversion is within this low-velocity layer for the events in the upper seismic plane.

The assumption (3) comes from the fact that the upper seismic plane below 100 km depth coincides with the UBP (Hasegawa *et al.* 1978b), and that almost all the events used here are deeper than 100 km. The events located above the UBP extrapolated from the result of each step of the inversion are excluded in the subsequent iteration. We do not consider the *P* to *S* conversion at the UBP from the refracted *P*-wave passing through the high-velocity lower layer for the events in the upper seismic plane (see Fig. 12c), because the amplitude of this converted wave is expected to be very small.

The UBP below about 100 km depth cannot be located by the inversion because all the stations on the western side of the volcanic front do not detect the *PS*-wave. We adopt an approximate calculation for the travel times between the stations and the events in the upper seismic plane below 100 km depth. In such a two-layered model, as shown in Fig. 12(a), the travel time of the refracted *P*-wave ($T_{\mathrm{ref}}^{\mathrm{AB}}$) from point A to point B in the figure is

$$
\begin{aligned}
T_{\mathrm{ref}}^{\mathrm{AB}} &= \frac{l_{1a}}{v_1} + \frac{l_{1b}}{v_2} + \frac{l_{1c}}{v_1} \\
&= \frac{l_0}{v_2} + \frac{2d}{v_1}\cos\theta \\
&= \frac{1}{v_2}\left\{ l_0 + 2d\sqrt{2\alpha + \alpha^2} \right\} \\
&\approx \frac{l_0}{v_2} + \frac{2d\sqrt{2\alpha}}{v_2} \qquad (\because \alpha \ll 1) \\
&= t_2^{\mathrm{AB}} + d\sqrt{2\alpha}\left(\frac{1}{v_2} + \frac{1}{v_2}\right), \qquad (2)
\end{aligned}
$$

where

$$
\alpha = \frac{1}{\sin\theta} - 1 = \frac{v_2}{v_1} - 1,
$$

d = thickness of the upper layer,

t_2^{AB} = travel time from point A to point B assuming that the velocity in the upper layer is the same as that in the lower layer,

Downloaded from https://academic.oup.com/gji/article/86/3/767/614858 by U.S. Department of Justice user on 17 August 2022

v_1, v_2 = velocities in the upper and the lower layers respectively ($v_1 < v_2$),

$l_{1a}, l_{1b}, l_{1c}, l_0, \theta$ = see Fig. 12(a).

If the boundary between these layers is gently curved and the velocity in each layer changes gradually with depth, the approximate travel time of the refracted wave from point A to B in Fig. 12(b) is expressed by modifying (2),

$$T_{\mathrm{ref}}^{\mathrm{AB}} \approx t_2^{\mathrm{AB}} + d\sqrt{2\alpha}\left(\frac{1}{v_2^{\mathrm{A}}} + \frac{1}{v_2^{\mathrm{B}}}\right), \tag{2'}$$

where v_2^{A} and v_2^{B} are velocities in the lower layer at the depths of points A and B respectively.

If the location of the earthquake is at point A in Fig. 12(b), we can calculate the travel time of the refracted *P*-wave passing through A–A′–B′–B station as follows,

(1) assume that the upper layer has the same velocity as in the lower layer and calculate the travel time T' using this velocity structure model,

(2) calculate the correction term T_{c}

$$T_{\mathrm{c}} = d\sqrt{2\alpha}\left(\frac{1}{v_2^{\mathrm{A}}} + \frac{1}{v_2^{\mathrm{B}}}\right), \tag{3}$$

(3) by adding T' and T_{c}, we have the travel time of the refracted wave (T_{ref})

$$T_{\mathrm{ref}} = T' + T_{\mathrm{c}}. \tag{4}$$

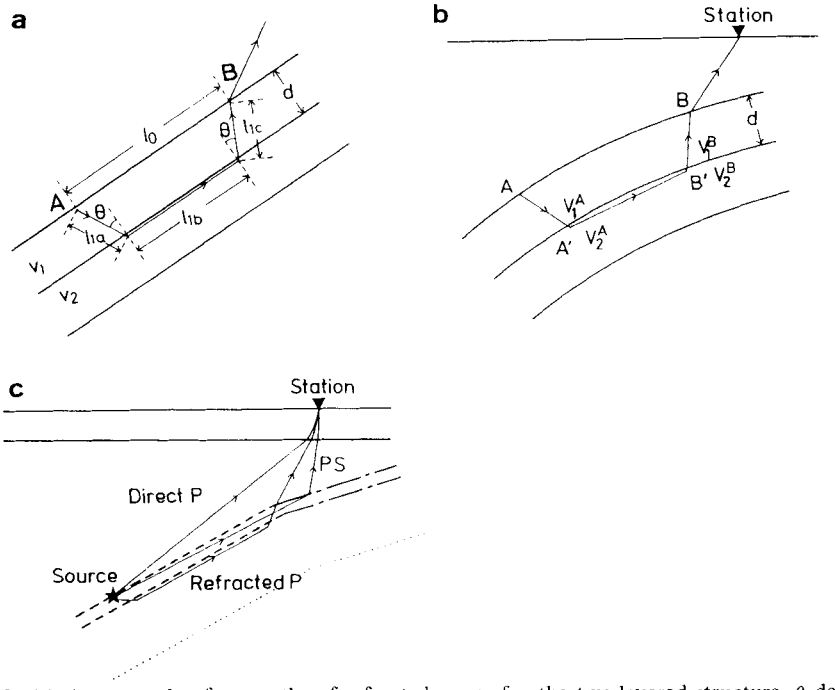

Figure 12. (a) An example of ray paths of refracted waves for the two-layered structure. θ denotes the incident angle at the inner boundary. (b) An example of ray paths of refracted waves for the gently curved layer model. (c) Ray paths assumed for the calculation of the travel times of the intermediate-depth earthquakes. Dot–dash lines denote the UBP and the internal boundary of the descending oceanic plate obtained by the inversion.

Downloaded from https://academic.oup.com/gji/article/86/3/767/614858 by U.S. Department of Justice user on 17 August 2022

The direct *P*-wave travel time (T_{dir}) for the event in the upper seismic plane below 100 km depth is calculated under the assumption that the location of the UBP is just above the event; and the smaller one between T_{dir} and T_{ref} is adopted as the real travel time of the *P*-wave (Fig. 12c). The travel time of the *PS*-wave for the event in the upper seismic plane is calculated assuming that this wave does not pass through the high-velocity lower layer. The total *PS*–*P* time error from this approximate calculation and the effect of fixing the hypocentre is estimated to be at most 0.2 s when the thickness of the low-velocity layer is 5 km and the velocity contrast is −6 per cent for the upper layer and 6 per cent for the lower layer. We do not use the data of events occurring on the western side of 140°E because the hypocentres of these events are scattered and the separation of hypocentres into the upper and the lower seismic planes is not clear.

In order to obtain the velocity contrasts for the two layers, we locate the UBP with various values of the velocity contrast and investigate which set of the velocity contrasts make the error minimum for the events both in the upper and the lower seismic planes. The results are shown in Fig. 13. The model in which the velocity contrast for the upper layer is −6 per cent and that for the lower layer is 6 per cent is the most appropriate because this model well explains the error of the *PS*–*P* time for the events both in the upper and the lower planes. Whether the thickness of the low-velocity layer is 5 or 10 km, the difference

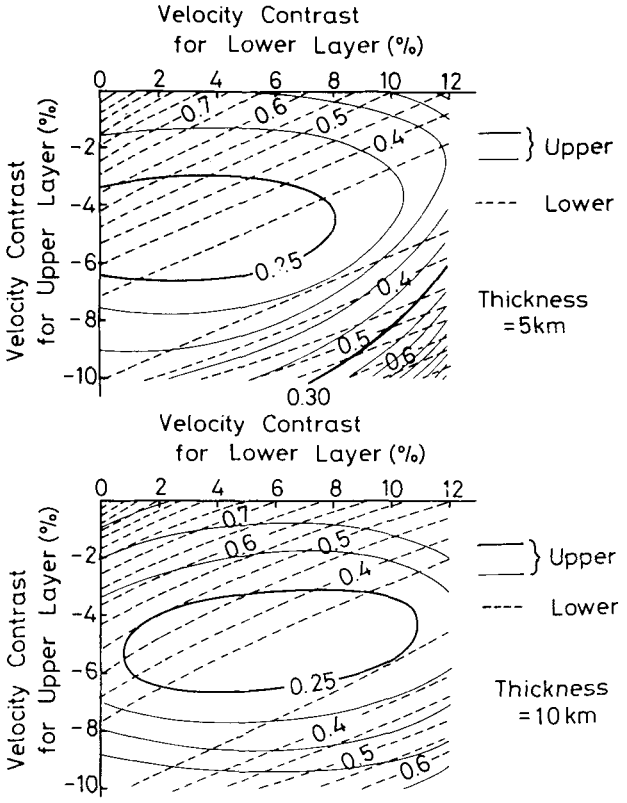

Figure 13. Standard deviation of the *PS*–*P* time residuals as a function of the velocity contrasts in the upper and lower layers. Contours shown by solid lines and dashed lines denote the standard deviations for the events in the upper seismic plane and in the lower seismic plane, respectively. Two cases in which the thicknesses of the low-velocity layer are 5 and 10 km are represented.

Downloaded from https://academic.oup.com/gji/article/86/3/767/614858 by U.S. Department of Justice user on 17 August 2022

in the depth to the UBP between the two is only 0.2 km at the central point of the stations (39.3°N, 141.8°E).

The geometry of the UBP determined by the inversion is shown in Fig. 14. Only the areas where conversion from *P* to *S* occurs is shown here, the standard deviation of the estimated depth to the UBP is less than 1 km in this area. The location of the UBP obtained here and that obtained by Hasegawa *et al.* (1978b) are shown together in Fig. 15. In this calculation, the thickness of the low-velocity layer is assumed to be 5 km and the velocities in the upper and the lower layers are assumed to be −6 and 6 per cent higher than the overlying mantle, respectively. In this model, the standard deviation of the *PS*–*P* time residual is 0.25 s for the events in the upper plane and 0.33 s for the events in the lower plane as shown in Fig. 13. These errors are comparable to the reading error which is estimated to be 0.3 s. The comparison of the observed *X*–*P* time with the calculated *PS*–*P* time is shown in Fig. 16.

The result obtained by the inversion shows that:

(1) the location of the UBP is just above the upper plane of the double-planed deep seismic zone, which is consistent with the assumption we adopted for the calculation of the travel time,

(2) the isobath of the UBP is almost parallel to the trench axis, and

(3) the dip angle of the UBP inverted in this study is slightly smaller than that inverted by using the *ScSp*-phase.

5 Two-layered oceanic plate model with gently curved form

In order to investigate the form of the UBP covering a wider area, we add the *PS*–*P* time data observed at stations HMK, HSK and KNK. In this case, we assume that the shape of the

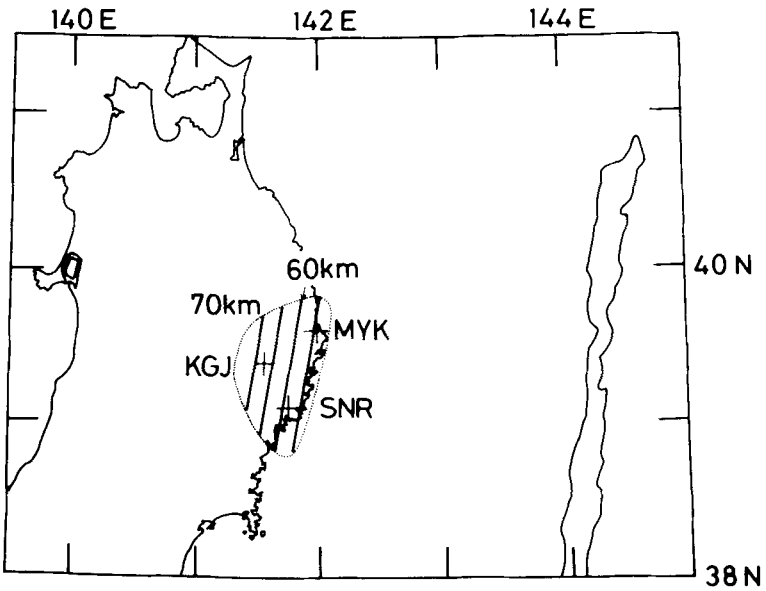

Figure 14. Contours of the depth to the UBP obtained from the inversion by assuming a two-layered structure for the descending oceanic plate. The dotted line represents the area where the conversion point of the *PS*-wave at the UBP is distributed. The standard deviation of the estimated depth to the UBP is less than 1.0 km within this area.

Downloaded from https://academic.oup.com/gji/article/86/3/767/614858 by U.S. Department of Justice user on 17 August 2022

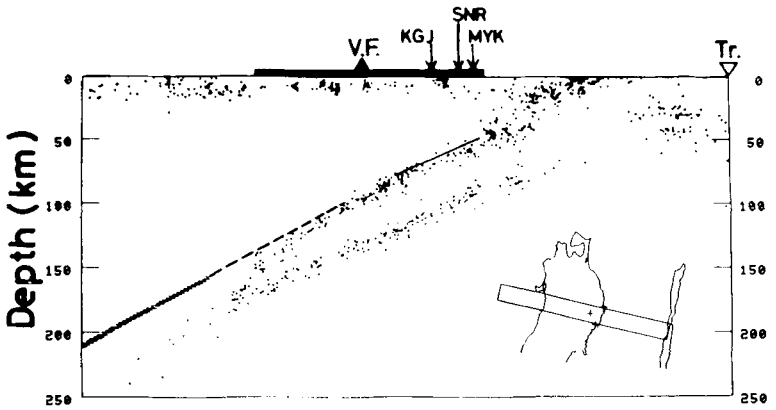

Figure 15. Location of the UBP (solid line) obtained by assuming the two-layered oceanic plate model. *PS–P* time data recorded at the three seismic stations are used. The location of the UBP obtained by using the *ScSp*-phase (hatched line) and that obtained by using the travel-time anomaly at the small-scale seismic array (dashed line) are also shown (after Hasegawa *et al.* 1978b). The locations of the land area, the volcanic front, the trench axis and the stations used for locating the UBP are shown by a thick line, a solid triangle, an open triangle and arrows, respectively.

UBP is expressed as

$$h_P = C_0 + C_1\,\phi'_P + C_2\,\lambda'_P + C_3\,\phi'^2_P + C_4\,\phi'_P\,\lambda'_P + C_5\,\lambda'^2_P, \tag{5}$$

because we can now use six unknown parameters. The inversion technique and the method of the travel-time calculation are the same as described in the previous section.

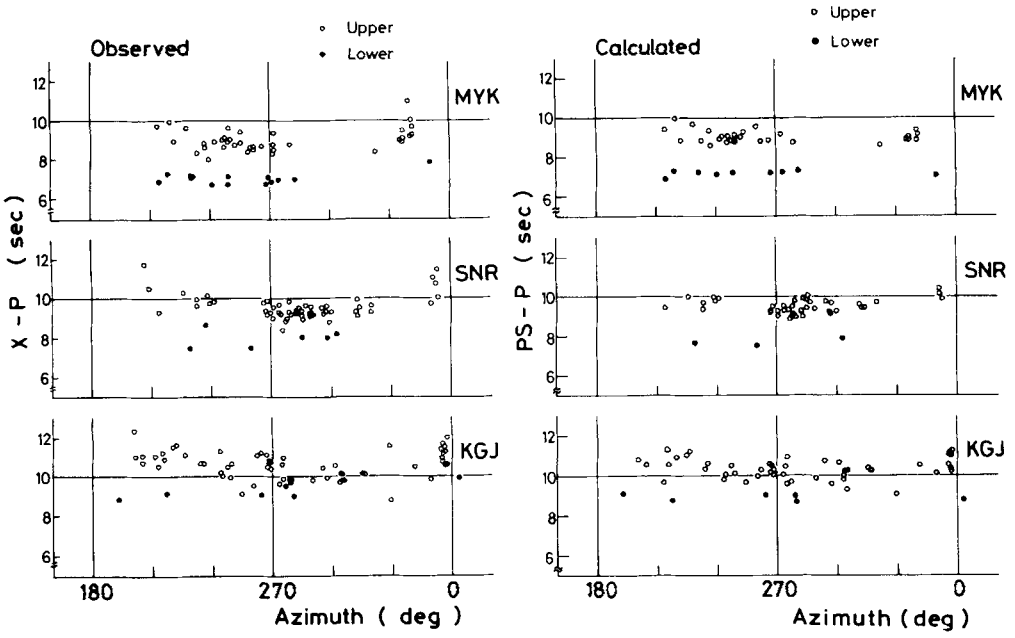

Figure 16. Azimuthal distribution of the observed *X–P* time (a) and the calculated *PS–P* time (b) for the two-layered oceanic plate model. Azimuths are measured clockwise from the north. Open and solid circles represent the events in the upper and lower seismic planes, respectively.

Downloaded from https://academic.oup.com/gji/article/86/3/767/614858 by U.S. Department of Justice user on 17 August 2022

Fig. 17 represents the geometry of the UBP obtained by this inversion. The contours of the depth to the UBP are nearly parallel to the trench axis except in the northern part, where they are slightly changed and are almost N–S. This feature of the UBP is similar to that of the upper seismic plane (see fig. 5 in Umino & Hasegawa 1982).

The UBP located is also shown in Fig. 18, where the UBP and seismicity are projected on to vertical sections. It is clear that the UBP is located just above the upper seismic plane in the region from 38.0°E to 40.5°E and in the depth range from 55 to 85 km. The *PS–P* time residuals (observed time–calculated time) are shown in Fig. 19. Almost all of the residuals for the six stations are within reading error (0.3 s) and systematic trends scarcely remain in the distribution of the residuals. We must point out that the data for stations HMK and KNK are rather poorer than those for other stations. The *PS*-phase is hardly observed at HMK because it is located near the volcanic front; and KNK sometimes has noisy data because it is very close to the sea. Therefore, the locations of the UBP near these two stations are somewhat vague.

6 Discussion

Hasegawa *et al.* (1978b) reveal that the UBP coincides with the upper seismic plane of the deep seismic zone below 100 km depth. The location of the UBP obtained in this paper is also just above the upper seismic plane in the depth range from 55 to 85 km. These results indicate that the upper seismic plane represents the shape of the UBP in the depth range at least from 60 to 150 km.

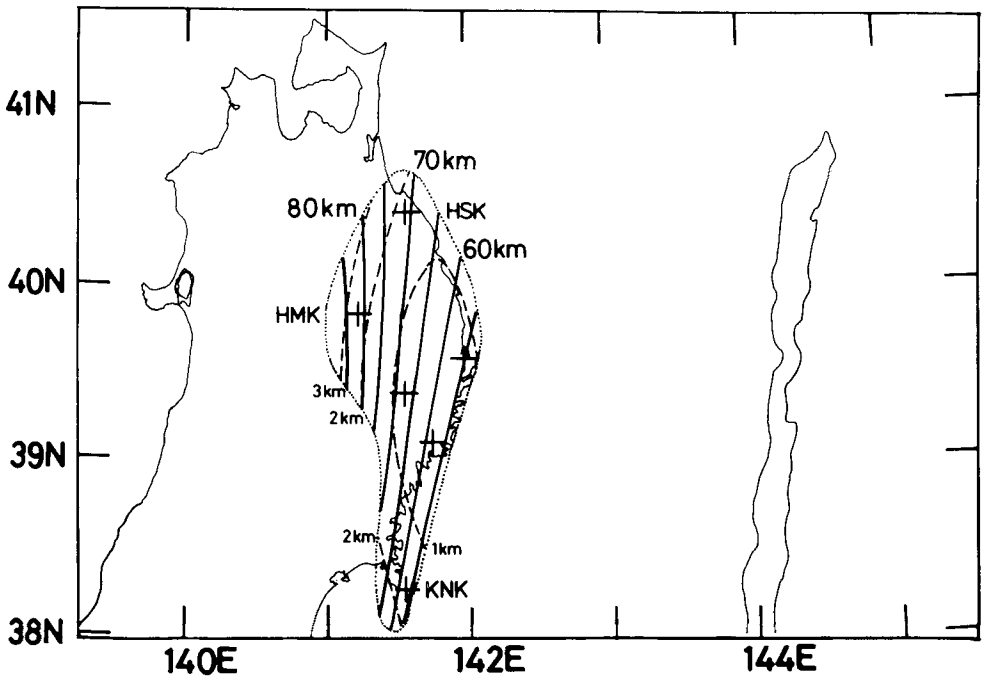

Figure 17. Contours of the depth of the UBP (solid lines) obtained from the inversion by using the *PS–P* time data at the six stations (crosses). The two-layered structure of the oceanic plate is assumed for locating the UBP. The dotted line represents the area where the conversion point of the *PS*-wave at the UBP is distributed. Dashed lines denote the standard deviation of the estimated depth to the UBP.

Downloaded from https://academic.oup.com/gji/article/86/3/767/614858 by U.S. Department of Justice user on 17 August 2022

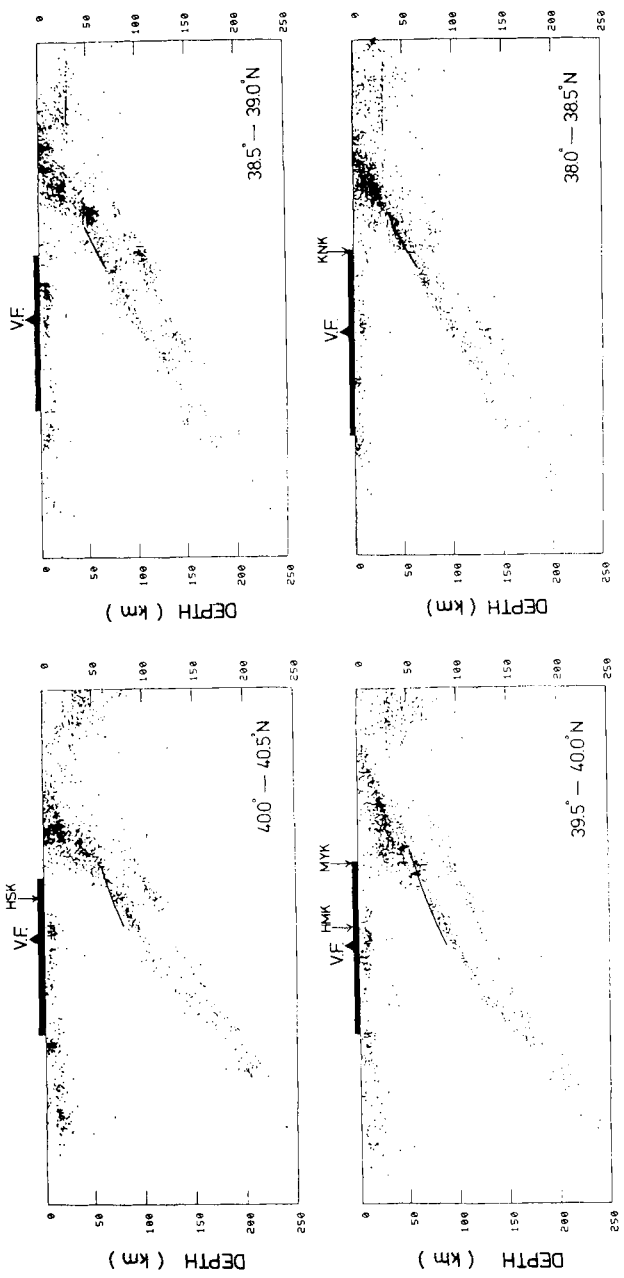

Figure 18. Vertical cross-sections of the UBP obtained by using the *PS*–*P* time data at the six stations. The two-layered velocity structure is assumed for the oceanic plate. The location of the UBP is denoted by a solid line. The locations of the land area, the volcanic front and the seismic stations used are denoted by a thick line, a solid triangle and arrows, respectively.

Downloaded from https://academic.oup.com/gji/article/86/3/767/614858 by U.S. Department of Justice user on 17 August 2022

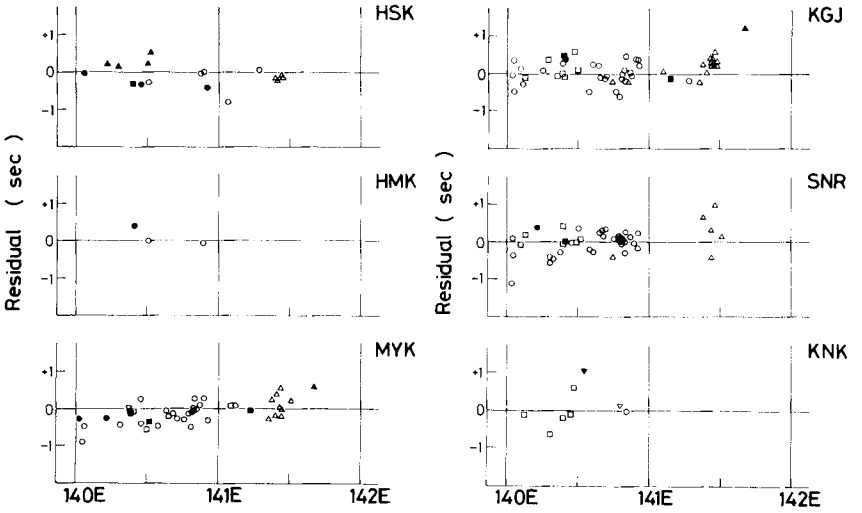

Figure 19. Residuals of the *PS–P* time for the six stations. Open and solid symbols denote the events in the upper and lower seismic planes, respectively. The abscissa is the longitude of the hypocentre. The latitude of the hypocentre is as follows. △, 40–41°N; ○, 39–40°N; □, 38–39°N; ▽, 37–38°N.

In order to explain the difference in the *PS–P* time between the events in the upper seismic plane and those in the lower plane, we have assumed that the descending oceanic plate is composed of two layers; upper and lower layers have −6 and 6 per cent higher velocities than the overlying mantle, respectively. The calculated *PS–P* time from this model agrees well with the observed one. Matsuzawa *et al.* (1986b) calculate the synthetic waveform of the *PS*-phase; and they ascertain that the two-layer model can explain the large amplitude of this phase. One may think that the sign of the velocity contrast can be determined if we check the relative polarity of the *PS*-phase as Nakanishi (1980) did. It is difficult, however, to check it because the onset of the *PS*-phase is not so sharp and we do not know the focal mechanism of the event; most of the seismograms of the events whose focal solution can be determined are saturated and we cannot pick up the *PS*-phase. Okada (1979) and Nakanishi (1980) also introduce the low-velocity layer intervening between the descending oceanic plate and the overlying mantle in order to explain the large amplitude of the *ScSp*-phase. Thus the existence of a thin low-velocity layer is probably a common feature beneath north-eastern and south-western Japan.

Although Hasemi *et al.* (1984) investigated the velocity structure beneath the Tohoku District by using the damped least squares method, they could not detect the low-velocity layer at the surface of the descending oceanic plate. Their resolving power of the inversion is about 30 km because of the limitation of the block size. Therefore, the thickness of the low-velocity layer is considered to be less than 10 km. This thin low-velocity layer may be related to the fact that large intermediate-depth earthquakes with magnitudes greater than 5 seldom occur in the upper seismic plane below 60 km depth.

Hori *et al.* (1985) found a clear later phase in the record of the subcrustal earthquakes in the Kinki District, the south-western part of Honshu, Japan. They conclude that this phase is a guided wave travelling within the low-velocity layer in the oceanic plate because this wave has a very low apparent velocity and large amplitude. In the Kinki District, the descending oceanic plate is directly in contact with the crust in the land area. Therefore if earthquakes occur in the low-velocity layer, the guided wave is likely to be observed at the stations in

Downloaded from https://academic.oup.com/gji/article/86/3/767/614858 by U.S. Department of Justice user on 17 August 2022

land area. In the Tohoku District, on the contrary, the depth to the descending oceanic plate is more than 60 km in land area. Even if the low-velocity layer exists in the oceanic plate, the guided wave cannot be observed at the stations in land area. Hori *et al.* (1985) conclude that this low-velocity layer is the oceanic crust descending with the oceanic plate. The inclined low-velocity zones where seismicity is very active are also found in Pamir–Hindu Kush (Roecker 1982) and in Hokkaido (Miyamachi & Moriya 1984). These low-velocity zones are also interpreted as the descending crust.

It is reported from experimental study that if the oceanic crust descends, gabbro will change into eclogite (e.g. Ringwood & Green 1966). Then the descending oceanic crust does not have a low velocity compared with the overlying mantle. However, Sacks (1983) insists that the speed of the phase change is quite small if the temperature in the descending oceanic plate is sufficiently low. The descending rate of the Pacific plate beneath the Tohoku District is high and is 10–11 cm yr^{-1} (Minster & Jordan 1978). Moreover, the plate is very old and presumably very cold. Thus the velocity within the descending crust is probably still low down to a considerable depth although there is no other strong support for our hypothesis so far as we know. The descending plate in the Tohoku District is older and hence less buoyant than the one beneath central Peru; therefore subducting of the plate is possible even if the phase change does not occur.

One may suppose that the partial melting of the overlying mantle is the cause of the low-velocity layer. We do not think, however, that earthquakes can occur in such a partially melting layer. This low-velocity layer must have a considerably high Q-value because the amplitude of the *PS*-wave which passes through this layer before conversion is quite large. It is impossible that the partially melting layer satisfies this condition. Therefore the low-velocity layer is considered to be the descending oceanic crust.

The *PS*-wave is also observed in other areas (e.g. Mitronovas & Isacks 1971; Reyners & Coles 1982). There are no confusing phases near the arrival time of the *PS*-wave in the horizontal component of the seismogram. Thus the *PS*-wave will be a powerful means to investigate the upper mantle velocity structure beneath subduction zones.

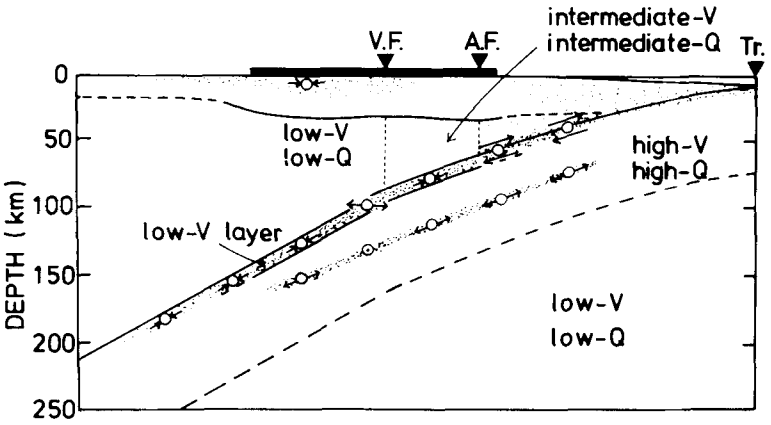

Figure 20. Schematic representation of the estimated upper mantle structure beneath the Tohoku District. The results obtained by previous studies (Umino & Hasegawa 1975; Hasegawa *et al.* 1978a, b, 1979, Matsuzawa *et al.* 1986a) are also included. Open circles with arrows denote the dominant focal mechanisms of the intermediate-depth earthquakes. The dotted area indicates the deep seismic zone. V.F., A.F. and Tr. represent the volcanic front, the aseismic front and the trench axis respectively.

Downloaded from https://academic.oup.com/gji/article/86/3/767/614858 by U.S. Department of Justice user on 17 August 2022

7 Conclusion

The upper boundary of the oceanic plate (UBP) in the depth range between 55 and 85 km is located by using the *PS*-wave (converted from *P* to *S* at the UBP). In order to explain the difference in *PS*–*P* time between the events in the upper seismic plane and those in the lower seismic plane, we introduce the two-layered oceanic plate model composed of a thin low-velocity upper layer and a thick high-velocity lower layer; the upper layer and the lower layer respectively have 6 per cent lower and 6 per cent higher velocity than the overriding mantle.

The obtained location of the UBP is just above the upper seismic plane of the deep seismic zone. This result is the same as the result of Hasegawa *et al.* (1978b) who located the UBP below 100 km depth by using the *ScSp*-phase. These facts indicate that the shape of the upper seismic plane delineates the UBP and that the events in the upper seismic plane occur within the thin low-velocity layer. The estimated upper mantle structure beneath the Tohoku District is shown schematically in Fig. 20.

Acknowledgments

We wish to express our sincere appreciation to Professor T. Hirasawa for his advice and to Dr H. Shimizu, Mr K. Obara and Mr M. Nosaka for their stimulating discussions. Thanks are also due to the members of the Observation Centre for Earthquake Prediction, the Aobayama Seismological Observatory, the Akita Geophysical Observatory, the Honjo Seismological Observatory, the Kitakami Seismological Observatory and the Sanriku Geophysical Observatory of Tohoku University, for valuable discussions.

References

Hasegawa, A., Umino, N. & Takagi, A., 1978a. Double-planed structure of the deep seismic zone in the northeastern Japan Arc, *Tectonophys.*, **47**, 43–58.

Hasegawa, A., Umino, N. & Takagi, A., 1978b. Double-planed deep seismic zone and upper-mantle structure in the northeastern Japan Arc, *Geophys. J. R. astr. Soc.*, **54**, 281–296.

Hasegawa, A., Umino, N., Takagi, A. & Suzuki, Z., 1979. Double-planed deep seismic zone and anomalous structure in the upper mantle beneath northeastern Honshu (Japan), *Tectonophys.*, **57**, 1–6.

Hasemi, A. H., Ishii, H. & Takagi, A., 1984. Fine structure beneath the Tohoku district, northeastern Japan arc, as derived by an inversion of *P*-wave arrival times from local earthquakes, *Tectonophys.*, **101**, 245–265.

Hori, S., Inoue, H., Fukao, Y. & Ukawa, M., 1985. Seismic detection of the untransformed 'basaltic' oceanic crust subduction into the mantle, *Geophys. J. R. astr. Soc.*, **83**, 169–197.

Horiuchi, S., Ishii, H. & Takagi, A., 1982. Two-dimensional depth structure of the crust beneath the Tohoku District, the northeastern Japan arc. Part I. Method and Conrad discontinuity, *J. Phys. Earth*, **30**, 47–69.

Matsuzawa, T., Umino, N., Hasegawa, A. & Takagi, A., 1986a. Normal fault type events in the upper plane of the double-planed deep seismic zone beneath the northeastern Japan Arc, *J. Phys. Earth*, submitted.

Matsuzawa, T., Umino, N., Hasegawa, A. & Takagi, A., 1986b. Synthetic *PS*-phase for the intermediate-depth earthquakes beneath the Tohoku District, in preparation.

Minster, J. B. & Jordan, T. H., 1978. Present-day plate motions, *J. geophys. Res.*, **83**, 5331–5354.

Mitronovas, W. & Isacks, B. L., 1971. Seismic velocity anomalies in the upper mantle beneath the Tonga–Kermadic island arc, *J. geophys. Res.*, **76**, 7154–7180.

Miyamachi, H. & Moriya, T., 1984. Velocity structure beneath the Hidaka Mountains in Hokkaido, Japan, *J. Phys. Earth*, **32**, 13–42.

Nakanishi, I., 1980. Precursors to *ScS* phases and dipping interface in the upper mantle beneath southwestern Japan, *Tectonophys.*, **69**, 1–35.

Downloaded from https://academic.oup.com/gji/article/86/3/767/614858 by U.S. Department of Justice user on 17 August 2022

Nakanishi, I., Suyehiro, K. & Yokota, T., 1981. Regional variations of amplitudes of *ScSp* phases observed in the Japanese Islands, *Geophys. J. R. astr. Soc.*, **67**, 615–634.

Okada, H., 1971. Forerunners of *ScS* waves from nearby deep earthquakes and upper mantle structure in Hokkaido, *Zisin. Ser. II*, **24**, 228–239 (in Japanese).

Okada, H., 1979. New evidence of the discontinuous structure of the descending lithosphere as revealed by *ScSp* phase, *J. Phys. Earth*, **27**, Suppl., S53–S63.

Reyners, M. & Coles, K. S., 1982. Fine structure of the dipping seismic zone and subduction mechanics in the Shumagin Islands, Alaska, *J. geophys. Res.*, **87**, 356–366.

Ringwood, A. E. & Green, D. H., 1966. An experimental investigation of the gabbro-eclogite transformation and some geophysical implications, *Tectonophys.*, **3**, 383–427.

Roecker, S. W., 1982. Velocity structure of the Pamir–Hindu Kush region: possible evidence of subducted crust, *J. geophys. Res.*, **87**, 945–959.

Sacks, I. S., 1983. The subduction of young lithosphere, *J. geophys. Res.*, **88**, 3355–3366.

Snoke, J. A., Sacks, I. S. & Okada, H., 1977. Determination of the subducting lithosphere boundary by use of converted phases, *Bull. seims. Soc. Am.*, **67**, 1015–1060.

Umino, N. & Hasegawa, A., 1975. On the two-layered structure of deep seismic plane in northeastern Japan Arc, *Zisin, Ser. II*, **28**, 125–139 (in Japanese).

Umino, N. & Hasegawa, A., 1982. A detailed structure of the deep seismic zone and earthquake mechanism in the northeastern Japan Arc, *Zisin. Ser. II*, **35**, 237–257 (in Japanese).

Appendix: the method of locating the UBP by using the *PS–P* time

It is assumed that the configuration of the UBP can be expressed by a polynomial of latitude and longitude,

$$h_P = C_{00} + C_{10}\phi'_P + C_{01}\lambda'_P + C_{20}\phi'^2_P + C_{11}\phi'_P\lambda'_P + C_{02}\lambda'^2_P + \ldots$$

$$= \sum_{k=0} \sum_{l=0} C_{kl}\,\phi'^k_P\,\lambda'^l_P, \tag{A1}$$

where ϕ'_P and λ'_P are the differences respectively in latitude and in longitude between any point and the centre of the stations. h_P is the depth of the UBP at the point and C_{kl} is an unknown parameter. If the curvature of the UBP is sufficiently gentle, its shape can be expressed by only lower-order terms of (A1).

When C_{kl} is determined, the location of the point where a ray crosses the boundary can be solved numerically. Travel time T and partial derivative $\partial T/\partial h_P$ can then be solved. The

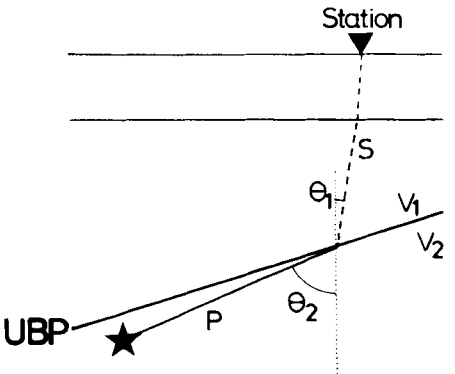

Figure A1. Ray path for the *PS*-wave projected on the vertical section.

Downloaded from https://academic.oup.com/gji/article/86/3/767/614858 by U.S. Department of Justice user on 17 August 2022

difference between the observed and calculated $PS-P$ time T_{PS-P} is expressed as follows:

$$T^{\text{obs}}_{PS-P} - T^{\text{cal}}_{PS-P} = \left(\frac{\partial T_{PS}}{\partial \phi_E} - \frac{\partial T_P}{\partial \phi_E} \right) \Delta\phi_E + \left(\frac{\partial T_{PS}}{\partial \lambda_E} - \frac{\partial T_P}{\partial \lambda_E} \right) \Delta\lambda_E + \left(\frac{\partial T_{PS}}{\partial h_E} - \frac{\partial T_P}{\partial h_E} \right) \Delta h_E + \sum_k \sum_l \left(\frac{\partial T_{PS}}{\partial C_{kl}} - \frac{\partial T_P}{\partial C_{kl}} \right) \Delta C_{kl} + e, \tag{A2}$$

where

T^{obs}_{PS-P} = the observed $PS-P$ time,

T^{cal}_{PS-P} = the calculated $PS-P$ time,

T_{PS} = calculated travel time of the PS-wave,

T_P = calculated travel time of the P-wave,

ϕ_E, λ_E, h_E = source parameters (latitude, longitude and depth respectively),

$\Delta\phi_E, \Delta\lambda_E, \Delta h_E$ = corrections of source parameters,

ΔC_{kl} = correction of unknown parameters,

e = error.

Since the coefficients of $\Delta\phi_E, \Delta\lambda_E, \Delta h_E$ in (A2) are very small (less than $0.02\,\text{s km}^{-1}$), we can neglect these terms. Then (A2) becomes

$$T^{\text{obs}}_{PS-P} - T^{\text{cal}}_{PS-P} = \sum_k \sum_l \left(\frac{\partial T_{PS}}{\partial C_{kl}} - \frac{\partial T_P}{\partial C_{kl}} \right) \Delta C_{kl} + e. \tag{A3}$$

The partial derivatives of T are

$$\frac{\partial T}{\partial C_{kl}} = \frac{\partial T}{\partial h_P} \frac{\partial h_P}{\partial C_{kl}} = \frac{\partial T}{\partial h_P} \phi_P'^k \lambda_P'^l, \tag{A4}$$

$$\frac{\partial T}{\partial h_P} = \frac{\cos\theta_1}{v_1} - \frac{\cos\theta_2}{v_2}, \tag{A5}$$

where v_1 and v_2 are the velocities just above and just beneath the UBP respectively; θ_1 and θ_2 are the emergent angle and the incident angle measured from the vertical (Fig. A1).

Equation (A3) can be written in matrix form as

$$\mathbf{d} = \mathbf{G}\mathbf{m} + \mathbf{e}, \tag{A6}$$

where $\mathbf{d}$ is a vector of the $PS-P$ time residual, $\mathbf{G}$ is a matrix of partial derivatives, $\mathbf{m}$ is a correction vector of unknown parameters and $\mathbf{e}$ is an error vector. Then, by the least squares method, we can obtain the correction vector

$$\mathbf{m} = (\mathbf{G}^{\mathrm{T}}\mathbf{G})^{-1}\mathbf{G}^{\mathrm{T}}\mathbf{d}. \tag{A7}$$

For the next step of iteration, $C_{kl} + \Delta C_{kl}$ is used in place of C_{kl} and thus C_{kl} is calculated repeatedly until ΔC_{kl} becomes sufficiently small.

Downloaded from https://academic.oup.com/gji/article/86/3/767/614858 by U.S. Department of Justice user on 17 August 2022